Available online at www.sciencedirect.com
ScienceDirect
Icarus 195 (2008) 131–139
ICARUS
www.elsevier.com/locate/icarus

The influence of van der Waals forces on the state of water in the shallow subsurface of Mars

Diedrich T.F. Möhlmann *

DLR Institut für Planetenforschung, Rutherfordstr. 2, D-12489 Berlin, Germany

Received 15 January 2007; revised 20 August 2007

Available online 3 January 2008

Abstract

Microscopic liquid layers of water can evolve via adsorption on grain and mineral surfaces at and in the soil of the surface of Mars. The upper parts of these layers will start to freeze at temperatures clearly below the freezing point of bulk water (freezing point depression). A sandwich structure with layers of ice (top), liquid water (in between) and mineral surface (bottom) can evolve. The properties of the interfacial water (of adsorption water and premelted ice) on grain surfaces are described by a sandwich-model of a layer of liquid-like adsorption water between the adsorbing mineral surface layer and an upper ice layer. It is shown that the thickness or number of mono-layers of the interfacial water (of adsorption water and premelted ice) depends on temperature and atmospheric relative humidity. The derived equations for the sandwich model fit well to a known phenomenological relation between thickness of the liquid layer and relative humidity, and can be a tool to estimate or to determine for appropriate materials Hamaker's constant for van der Waals interactions on grains and in porous media. The curvature of grain surfaces is shown to have no remarkable effects for particles in the μm-range and larger. The application of these equations to thermo-physical conditions on Mars shows that the thickness of frost-layers, which can evolve over several hours on cooling surface parts of Mars, is typically of the order or a few tenths of one millimeter or less. This is in agreement with observations. Furthermore, an equation is derived, which relates the freezing point depression for van der Waals force governed interfacial water to the value of the Hamaker constant, to the latent heat of solidification, to the mass density of water ice, and to the thickness of the liquid-like layer. Again, this equation fits well to a known phenomenological relation between freezing point depression and thickness of the liquid-like layer. The derived equation shows that the lower limiting temperature of the liquid phase can reach about 180 K under martian conditions having an atmospheric water content of around 10 pr μm. An "Equilibrium Moisture Content" (EMC)/"Equilibrium Relative Humidity" (ERH) relation for the water content of martian soil has been derived, which relates, for equilibrium conditions, soil water content and atmospheric relative humidity. This relation indicates that the content of liquid interfacial water in the upper surface of Mars can reach up to 10% by weight and more in course of saturation during night hours, and it can be of about 2% by weight during the dry daytime hours.

Keywords: Mars, surface; Ices

1. Introduction

The presence of water vapor in the atmosphere and the prevailing thermal conditions on Mars indicate an at least temporary existence of adsorption water (Möhlmann, 2004) and interfacial water (of adsorption water and premelted ice). Ryan and Sharman (1981) have found indications for condensation and/or adsorption phenomena on Mars by detecting the frost point temperature level for this phase change of water vapor in the Viking temperature measurements. Landis et al. (in preparation) have by imaging directly shown the temporary existence of frost on the MER-Opportunity (cf. Fig. 1). These frost phenomena may be due to freezing (of at least the upper layers) of film-like adsorption water. This "white frost" seems to be different from frost deposition phenomena, as observed by Viking (cf. Jones et al., 1979), which show fine frost-like condensates, which seem to have been blown over the surface.

More recently, results of the NASA mission Mars Odyssey and the ESA mission Mars Express have proven the exis-

* Fax: +49 30 67055 346.
E-mail address: dirk.moehlmann@dlr.de.

0019-1035/$ – see front matter
doi:10.1016/j.icarus.2007.11.026

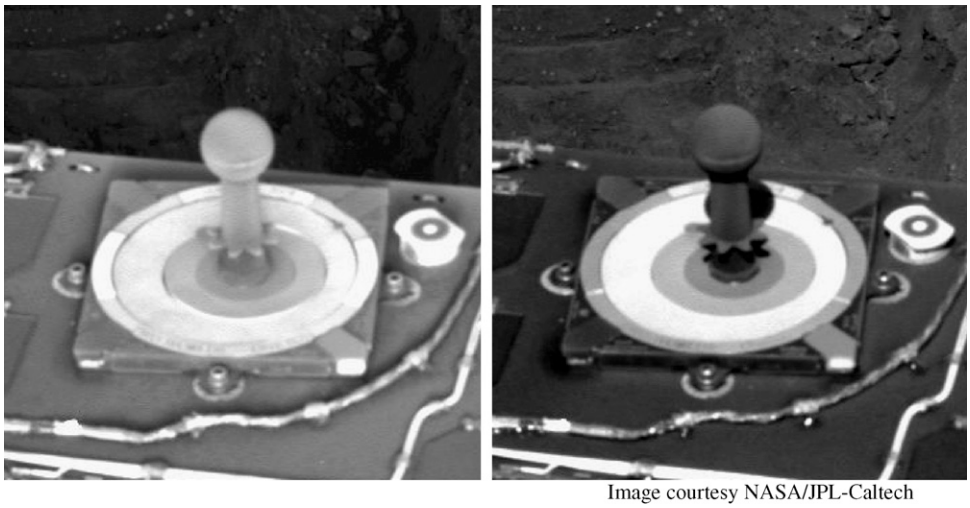

Image courtesy NASA/JPL-Caltech

Fig. 1. Frost (left image part) on the surface from the MER-B "Opportunity", at October 13, 2004 (morning of MER-B sol 257, short after aphelion, southern winter, $L_S = 100.5$). Local time: left image at 6:15—just after sunrise—right image at 9:22. The height of the frost layer seems to be less than 1 mm. Note that the surface of Mars (in the background) is not covered by frost. Source: Landis et al. (in preparation).

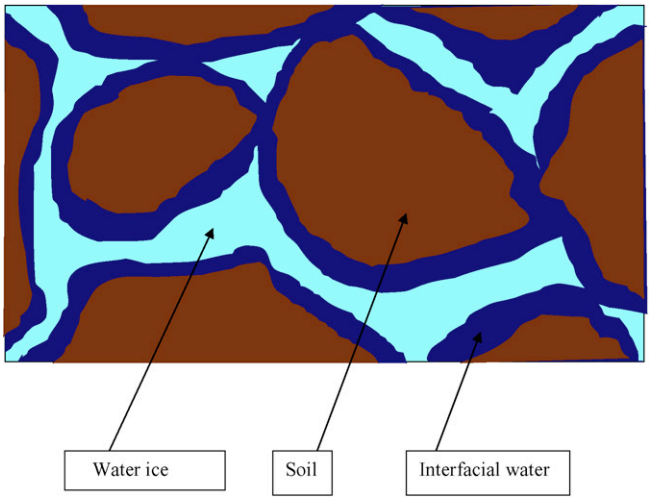

Fig. 2. Adsorption water and ice or capillary water in frozen wetted soil.

tence of water and water ice at and in the upper surface of Mars at both mid- and low-latitudes (Boynton et al., 2002; Feldman et al., 2002; Mitrofanov et al., 2002; Bandfield, 2007; Jouglet et al., 2007). It has to be mentioned, that the soil may harbor water also in the form of hydrated minerals and salts (Bish et al., 2003; Vaniman et al., 2004). The chemically bound water is more strongly attached, compared to interfacial water (of adsorption water and premelted ice—for a definition of premelted ice at the surfaces of solid ice see Dash et al., 2006), and it is not so freely available for physical (including rheological), chemical and eventual biological processes.

The existence of unfrozen water below standard freezing point temperatures of bulk water is a known fact in terrestrial soils (Anderson and Tice, 1972), specifically in permafrost soils (Ershov, 1998; Williams and Smith, 1989). Fig. 2 is a schematic drawing, which describes the coexisting water components, namely adsorbed water and ice in frozen, wetted soil. The interfacial water is in this case identical to the unfrozen water. At temperatures near to the melting point of bulk water, capillary water may become an additional water component, but this will not be studied in detail here.

The unfrozen water will be described in the following in terms of interfacial water. This water is in its dynamics governed by the action of van der Waals forces from the adsorbent (or adsorbing substrate). These allow the lower layers of interfacial water to remain liquid-like at temperatures far below the freezing point (cf. Farmer and Doms, 1979; Zent and Quinn, 1997; Jakosky et al., 2003). This can be of importance for potential physical and (photo-driven) chemical and potentially even for biological processes (Möhlmann, 2005).

The upper mono-layers of adsorbed water as one component of interfacial water are not so directly influenced by the van der Waals forces from the adsorbent, they increasingly accrue properties of capillary and bulk water with the onset of freezing at 0 °C. The mobility of adsorbed water molecules over the adsorbing grain surface arises due to diffusion over the adsorbing surface. Like a sandwich-structure, a liquid-like layer with molecular transport properties can remain in case of the presence of ice between the solid surfaces of ice and grain minerals. It has to be mentioned here, that an analogous model has been developed in terms of the premelting of ice (Wettlaufer and Worster, 2006; Dash et al., 2006). Premelted ice is due to the presence of water ice the other important component of interfacial water on Mars. A related sandwich-model of partially frozen interfacial water will in the following be the basis for a quantitative description of physical properties of the unfrozen or interfacial water in the surface soil of Mars (cf. Fig. 3).

2. The sandwich model of water on mineral surfaces

2.1. Plane parallel surfaces

The phenomenon of a liquid layer between water ice and a solid surface (of a mineral grain, e.g.) at temperatures below the freezing point is described in the literature (cf. Anderson and Tice, 1972; Williams and Smith, 1989, specifically also in terms

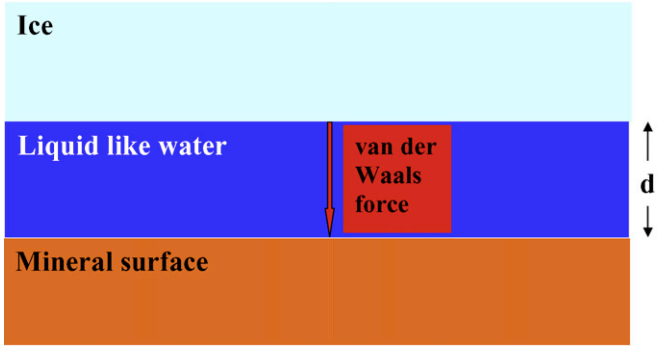

Fig. 3. Sandwich model of an adsorption water layer of thickness d between attracting surfaces of ice and adsorbent at temperatures below the freezing point. Note that there are two interfaces (or surfaces), i.e., ice/water, and water/mineral.

of liquid films of so-called premelted ice (Dash et al., 2006). Therefore, the model, as it is described here, is not restricted to water layers with an adsorption history only.

The van der Waals force per area S of two planar surfaces at a separation distance "d" is given by

$$\frac{F_{\mathrm{vdW}}}{S} = \frac{A_{132}}{6\pi d^3}, \tag{1}$$

where A_{132} is the Hamaker constant for the interaction of substances "1" and "2" in presence of medium "3" (Hamaker, 1937). This pressure is equivalent to the energy density $\varepsilon_{\mathrm{vdW}}$ of the van der Waals force within the layer of height d:

$$\varepsilon_{\mathrm{vdw}} = \frac{A_{132}}{6\pi d^3}, \tag{2}$$

and the bond energy per molecule is, with the molecule number density of the liquid N_L described by $\varepsilon_{\mathrm{vdW}}/N_L$.

The saturation pressure of water vapor at a planar ice surface can be described by $p_0 = ae^{-E_W/kT}$, with the constants $a = 3.47 \times 10^{12}$ Pa and $E_W = 8.4662 \times 10^{-20}$ J (Möhlmann, 2004). E_W is the bond energy per water molecule. Then, $\varepsilon_W = E_W N_L$ is the bond energy density of the water molecules on the ice-surface. The attraction on the water molecules by the van der Waals forces of the adsorbent weakens their bond on the ice surface. Correspondingly, in the sandwich model, the equilibrium water vapor partial pressure, p at the ice surface increases due to the counteracting presence of the planar mineral surface with the attracting van der Waals force:

$$p = ae^{-(\varepsilon_W - \varepsilon_{\mathrm{vdW}})/N_L kT}. \tag{3}$$

The water molecules at the ice/water interface can leave the ice more easily due to that attraction, and the liquid water layer will grow by capturing these water molecules after release from the ice.

The bond energy of water molecules on mineral surfaces can be much stronger in the case of hydrophilic minerals, compared to their bond to ice, as described above by E_W. Therefore, mineral surfaces can capture water more effectively than ice. In case of differences in the bond energies of 0.2 eV only (as between ice and montmorillonite), the bond is stronger by a large factor of $\exp(-(0.2\ \mathrm{eV})/(kT)) = 37{,}800$ for $T = 220$ K (cf. Möhlmann, 2004). This is the reason that interfacial water may have survived the continued sublimation processes of ices in the upper martian surface even over geological time scales (Möhlmann, 2004). It will be shown in Section 4.1, that, depending on the specific surface of the soil, the amount of interfacial water can reach up to a few percent by weight.

Equation (3) can be rewritten

$$a_W = \frac{p}{p_0} = e^{\frac{\varepsilon_{\mathrm{vdW}}}{N_L kT}}, \tag{4}$$

where $a_W = p/p_0$ is the so-called water activity. Equation (4) indicates for the sandwich-model that $p > p_0$. This approximation of plane boundary surfaces neglects surface energy due the curvature of grain surfaces, which can cause a further increase of the saturation pressure. This will be discussed in Section 2.3.

2.2. Thickness of mono-layers and the Hamaker constant

Equations (2) and (4) can be combined to give

$$N_L kT \left| \ln \frac{p}{p_0} \right| = \frac{A}{6\pi d^3}. \tag{5}$$

Here, for brevity, A is taken for the Hamaker constant, if no specific systems are under consideration. Then the thickness of the water film is, for equilibrium conditions, given by

$$d = \left(\frac{A/6\pi}{(\rho_{\mathrm{H_2O}}/m_{\mathrm{H_2O}})kT\,|\ln(p/p_0)|} \right)^{1/3}, \tag{6}$$

and the number $n = d/\delta$ of mono-layers (of thickness $\delta = 3.5 \times 10^{-10}$ m) is

$$n = \left(\frac{(A/6\pi)\delta^{-3}}{(\rho_{\mathrm{H_2O}}/\mathrm{m}_{\mathrm{H_2O}})kT\,|\ln(p/p_0)|} \right)^{1/3}. \tag{7}$$

Here, $\rho_{\mathrm{H_2O}}$ is the mass density of the liquid-like water layer, and $m_{\mathrm{H_2O}} = 3 \times 10^{-26}$ kg is the mass of the water molecule.

It is interesting to note that Wheeler (1955) has proposed the determination of the number n of mono-layers via:

$$n = \left(\frac{\bar{A}}{|\ln(p/p_0)|} \right)^{B}. \tag{8}$$

Sneck and Oinonen (1970) have experimentally found that $\bar{A} = 1.63$ and $B = 1/3$ (see also Fagerlund, 1973). Then, a Hamaker constant $A = 1.78 \times 10^{-19}$ J or 178 zJ (1 zJ $= 10^{-21}$ J, z—for "zepto") will numerically reproduce Eq. (7) in the case that the parameter $\bar{A} = 1.63$ has been determined for a temperature of 293 K. This is a comparatively high value of the Hamaker constant for systems interacting across water.

Characteristic thicknesses of the layers under consideration, as they follow with Eq. (8), are about one monolayer or less until the relative humidity approaches saturation ($a_W \geqslant 1$). About 10 monolayers (and more) are typical for $a_W \geqslant 0.99$. Condensation starts at $a_W = 1$.

Typical values of Hamaker's constant range for symmetrical systems ("1" = "2") between about 100 zJ and a few zJ (Fernandez-Varea and Garcia-Moliona, 2000; Ackler et al., 1996). Diamond is as strong as 130 zJ, while silica (SiO_2) is

of 4.3 zJ. Wilen et al. (1995) have calculated the Hamaker constants for different systems of substrate–water–substrate and ice–water–substrate with the result: "The typical Hamaker constant for two planar surfaces separated by a water layer is an order of magnitude larger than the corresponding value for an interface between ice and substrate." The derived values for ice–water–substrate systems are in the range of a few zJ to several tenths of a zJ. This large range of values characterizes the different wetting properties of different materials. Thus, a different content of adsorption water on and in the surface of Mars can be expected for sites of different mineralogy.

The above relations between layer-thickness, temperature, and water activity have been derived in a plausible way by using energetic relations. Alternatively, these relations can be derived by using the chemical potential as it is used in thermodynamics. This, for the van der Waals attraction is given by

$$\Delta\mu_{\mathrm{vdW}} = \Delta p/N = (p_s - p_l)/N = -A/(6\pi d^3 N_L). \tag{9}$$

The subscripts s and l correspond to the solid and liquid phases. For condensation of water vapor to the liquid phase, the chemical potential is

$$\Delta\mu_{\mathrm{cond}} = kT\ln(p/p_0). \tag{10}$$

The equilibrium condition $\Delta\mu_{\mathrm{vdW}} = \Delta\mu_{\mathrm{cond}}$ leads to Eq. (5).

2.3. Curved surfaces of soil grains

In soil, grain particles with their large specific surfaces can act as effective adsorbents. The model of plane surfaces described above will no longer be applicable in the case of sufficiently small grain radii, when the surface tension of the water film around the grain can become important. The corresponding energy density ε_C depends in this case on the surface tension σ [$\mathrm{N\,m^{-1}} = \mathrm{Ws\,m^{-2}}$], or the interfacial excess energy per unit area of the ice–water interface, and on the curvature κ of the grains. It is given by

$$\varepsilon_C = \sigma\kappa. \tag{11}$$

Here, the curvature corresponds to a surface point, which is to be characterized by two curvature radii R_1 and R_2. It is given then by $\kappa = 1/R_1 + 1/R_2$. In the case of a sphere of radius R, the curvature is $\kappa = 2/R$.

The related chemical potential is given by

$$\Delta\mu = \frac{\varepsilon_C}{N} = kT\ln p/p_0, \tag{12}$$

which, together with the critical radius $R_{\mathrm{crit.}}$

$$R_{\mathrm{crit.}} = \frac{\sigma}{NkT} \tag{13}$$

is equivalent to the Gibbs–Thomson equation

$$\frac{p}{p_{e,p}} = e^{R_{\mathrm{crit.}}\kappa}. \tag{14}$$

This illustrates that curved liquid surfaces exhibit a higher induced water vapor equilibrium pressure than plane surfaces. Therefore, the curvature-caused increase in the water vapor equilibrium pressure counteracts the release of water molecules from the ice. The sandwich-model for curved surfaces can analogously be described by

$$p = ae^{-(\varepsilon_W - \varepsilon_{\mathrm{vdW}} + \varepsilon_C)/N_L kT}. \tag{15}$$

The water activity and the number of mono-layers increase correspondingly for a granular soil of grains:

$$a_W = \frac{p}{p_0} = e^{(\varepsilon_{\mathrm{vdW}} - \varepsilon_C)/N_L kT}, \tag{16}$$

$$n = \left(\frac{(A/6\pi)\delta^{-3}}{(\rho_{\mathrm{H_2O}}/m_{\mathrm{H_2O}})kT|\ln(p/p_0)| + \sigma\kappa}\right)^{1/3}. \tag{17}$$

This dependence of the number n of monolayers on ware activity and curcature is described by Fig. 4. A comparison of the wetting-related energies due to the action of the van der Waals force and of the curvature of the liquid-surface leads to the result that these will become comparable for grain radii about 0.4 μm, when $d \approx 1$ nm, and $A \approx 100$ zJ. Thus, the wetting properties of micrometer sized (and smaller) particles are effectively reduced and limited by the Kelvin effect. This is due to the increasing equilibrium water vapor pressure for decreasing radii.

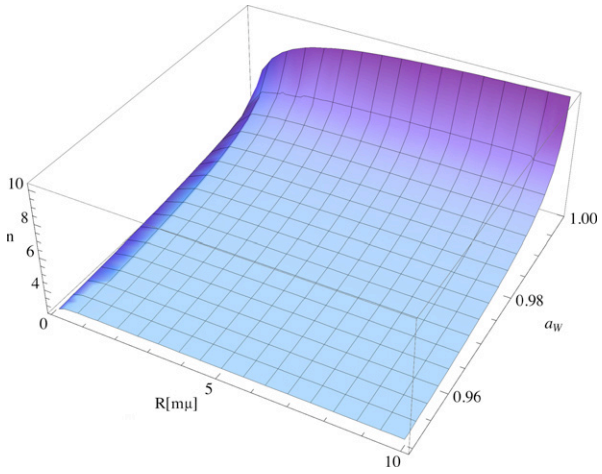

Fig. 4. Number n of "mono-layers" of the water film between ice and mineral surfaces plotted against water activity a_W and grain radius R [μm] for a Hamaker constant $A = 100$ zJ) and at $T = 220$ K.

2.4. Adsorption under martian conditions

The number of mono-layers of adsorbed water depends on water activity, as described by Eqs. (7) and (17). The water activity, a_W on Mars depends on temperature and relative humidity of the atmosphere, and the temperature depends on location and time of day. The diurnal profile of the water activity can be determined for known atmospheric water content and temperature. In the case of an average and diurnally constant 10 pr μm, as is typical for equatorial and mid-latitudinal regions (Smith, 2004), the number density of water molecules is 3×10^{19} $\mathrm{m^{-3}}$ at the surface. Fig. 5 shows the diurnal profile of the surface temperature, as used in the model-computations. It was taken for dust-free conditions from the Mars Climate Database (Jussieu-model, www-mars.lmd.jussieu.fr; Lewis et al., 1999), and it corresponds to the location of MER-Opportunity

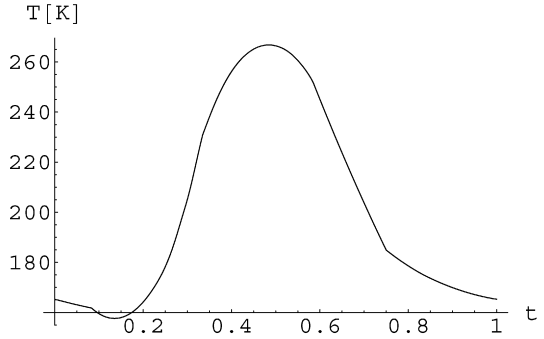

Fig. 5. Diurnal surface temperature profile, corresponding to the landing site of MER. Opportunity at $L_s = 60$–90 (southern winter, aphelion) (Mars Climate Database, Jussieu-model, www-mars.lmd.jussieu.fr; Lewis et al., 1999).

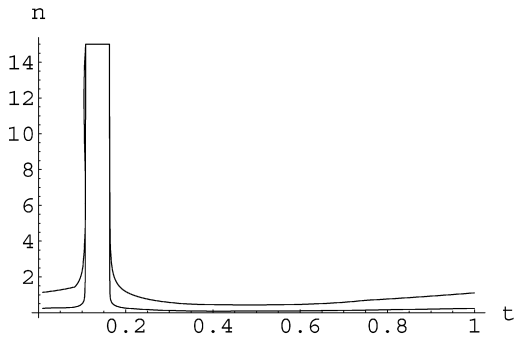

Fig. 6. Diurnal profile of the number of mono-layers $n(t)$ for a temperature profile, as described by Fig. 5, an atmospheric water content of 10 pr µm, for the Hamaker constants $A = 1$ zJ (lower curve) and $A = 100$ zJ, respectively, and for 1 µm sized grains. The constant n-value at late night hours indicates saturation (and related condensation) of water vapor, it is not a computed maximum value of n.

at aphelion conditions. Fig. 5 shows a typical diurnal temperature profile, which will be used for the following model calculations.

A graphical representation of the resulting diurnal $n(t)$-profiles over one martian day is described by Fig. 6, which describes the resulting diurnal variation of the number of "monolayers" in the film of liquid water, as follows from Eq. (7). Obviously, effective adsorption can take place at late night hours only.

Obviously, there are (seasonally changing) conditions on Mars including near equatorial latitudes, which favor adsorption and condensation processes at the martian surface (cf. Möhlmann, 2004). Of course, the related low temperatures will cause a partial freezing of that water. The resulting structure of this liquid water of the surfaces of mineral grains is described by the "sandwich-model" (cf. Section 1). During day-time, the content of adsorption water in the uppermost surface is reduced via desorption due to the comparatively warmer conditions, while deeper and cooler layers below the thermally active surface (with a diurnal temperature profile) may act as cold-traps and, in equilibrium with the atmospheric water content, accumulate and exchange water more steadily.

It can be seen from Fig. 6 that frost, shown in Fig. 1, could have evolved during late night by adsorption, followed by freezing of the upper water layers. The maximum thickness of the frozen frost layer depends on the duration of freezing, which is about 2 h (cf. Fig. 6). The increase in "height" h of the frost due to freezing can be described by $\mathrm{d}m/\mathrm{d}t = \rho_F F\,\mathrm{d}h/\mathrm{d}t$ for the mass change over a surface F:

$$\frac{\mathrm{d}h}{\mathrm{d}t} = \frac{m_{\mathrm{H_2O}}}{\rho_F}\frac{N v_{\mathrm{th}}}{4} = \frac{N}{\rho_F}\sqrt{\frac{m_{\mathrm{H_2O}} kT}{2\pi}}. \tag{18}$$

Here, a vertical mass flow rate (per surface area and time) $mNv_{\mathrm{th}}/4$ is taken, v_{th} is the thermal velocity of the water vapor molecules, and ρ_F is the mass density of the frost. The temperatures at the Opportunity landing site during the cold night hours at $L_S = 60$–90 are around 160 K. For an atmospheric water column content of 10 pr µm (corresponding to $N = 3 \times 10^{19}\ \mathrm{m^{-3}}$), sublimation is at these temperatures much weaker than freezing. The about 10 pr µm are typical for the region at $L_S = 60$–90 (Smith, 2004). It follows with $\rho_F = 900\ \mathrm{kg\,m^{-3}}$ that $\mathrm{d}h/\mathrm{d}t \approx 8 \times 10^{-8}\ \mathrm{m\,s^{-1}}$. Thus, about 0.5 mm of frost, or at least a few tenths of a millimeter can form within 2 h. This is compatible with Fig. 1, and with Viking observations of a very thin frost layer on the ground (Landis, 2007).

3. Freezing point depression

3.1. Gibbs–Thomson effect

As described in Section 2.3, the surface curvature of a liquid surface is related to vapor pressure and chemical potential (cf. Eq. (12)). Accordingly, the related Gibbs–Thomson equation (Eq. (14)) can, in the case of a characteristic curvature radius r be described by

$$\frac{p}{p_{e,p}} = e^{(2\sigma/NkT)(1/r)}. \tag{19}$$

Obviously, the water vapor pressure increases with decreasing curvature radii. The Gibbs–Duhem relationship (cf. Wood and Battino, 1990) is in this case given by

$$p_s - p_l = \Delta p = \varepsilon_C = \frac{2\sigma}{r} = \rho_{\mathrm{ice}} q \frac{T_m - T}{T_m} = \rho_{\mathrm{ice}} q \frac{\Delta T}{T_m}. \tag{20}$$

Here, T $(= T_l)$ is the limiting temperature of the liquid phase of the water layer below the bulk melting temperature T_m, and q is the latent heat of solidification per unit mass, ρ_{ice} is the ice mass density, and the subscripts s and l correspond to the solid and liquid phases.

The freezing point depression can be expressed as

$$\Delta T = T_m \frac{2\sigma/\rho_{\mathrm{ice}} q}{r}. \tag{21}$$

Numerically, it follows that

$$\Delta T\ [K] = \frac{0.05}{r\ [\mu\mathrm{m}]} \tag{22}$$

(having substituted: $\rho_{\mathrm{ice}} = 916.8\ \mathrm{kg\,m^{-3}}$, $q = 3.33 \times 10^5\ \mathrm{J\,kg^{-1}}$, $\sigma = 3 \times 10^{-2}\ \mathrm{N\,m^{-1}}$). The value of $0.05/r$ [µm] agrees with measurements of the freezing point depression of water (Liu et al., 2003). Obviously, the Gibbs–Thomson effect is only small for water films on micrometer-sized grain particles, but this can change for nanometer-sized structures.

3.2. Freezing point depression in the sandwich-model

Assuming that the sandwich-model (described above) of a plane and ice-covered liquid-like layer of height, d above the substrate surface with van der Waals forces is in local thermodynamic equilibrium, a consequence of the Gibbs–Duhem relationship (cf. Wood and Battino, 1990) is

$$p_s - p_l = \Delta p = \frac{A}{6\pi d^3} = \rho_{\text{ice}} q \frac{T_m - T}{T_m} = \rho_{\text{ice}} q \frac{\Delta T}{T_m}. \tag{23}$$

Obviously, the temperature of real melting/freezing decreases (or ΔT increases) with decreasing depth d of the liquid layer:

$$d = \left(\frac{A T_m}{6\pi \rho_{\text{ice}} q \Delta T}\right)^{1/3} \tag{24a}$$

or

$$n = \left(\frac{A T_m \delta^{-3}}{6\pi \rho_{\text{ice}} q \Delta T}\right)^{1/3} \tag{24b}$$

and

$$\Delta T = \frac{A T_m}{6\pi \rho_{\text{ice}} q d^3}. \tag{24c}$$

Thus, the real limiting temperature for the liquid phase of the "liquid-layer" layer is for $A = 100$ zJ, and in case of 1 "mono-layer" given by $T_l(n = 1) \approx 163$ K.

It is interesting to note that Fagerlund (1973) has suggested the relation

$$n = 5.628(1/\Delta T)^{1/3} \tag{25}$$

for the dependence of the number of mono-layers on the freezing point depression ΔT. The numerical factor has been derived by assuming that the diameter d of a water molecule is $d = 0.35$ nm. The related Hamaker constant follows by using Eqs. (24b) and (25) with $A = 161.5$ zJ. Here, $q = 3.33 \times 10^5$ J kg^{-1}, and $\rho_{\text{ice}} = 916.8$ kg m^{-3} have been used.

The value 161.5 zJ fits the values derived from Eqs. (7) and (8) surprisingly well. Thus, values of the order of 100 zJ seem to be realistic for wetted soils, at least under terrestrial conditions. There are no reasons to assume differences on Mars. Nevertheless, it is a current challenge to get more reliable data of Hamaker's constant for Mars-relevant minerals.

Equation (24a) gives, with Eq. (6):

$$\frac{\Delta T}{T_m} = \frac{(\rho_{\text{H}_2\text{O}}/m_{\text{H}_2\text{O}})}{\rho_{\text{ice}} q} kT \left|\ln\big(p(T)/p_0(T)\big)\right|. \tag{26}$$

The limiting temperature $T = T_l$ (where freezing starts) of the liquid phase of the water layer can implicitly be described by

$$T_l = T_m \left(1 - \frac{\rho_{\text{H}_2\text{O}}/m_{\text{H}_2\text{O}}}{\rho_{\text{ice}} q} kT_l \left|\ln\big(p(T_l)/p_0(T_l)\big)\right|\right). \tag{27}$$

In a real atmosphere and under equilibrium conditions, T_l depends accordingly on the density of the atmospheric water vapor. Fig. 7 describes this dependence for the values $T_m = 273$ K, $\rho_{\text{H}_2\text{O}} = 1000$ kg m^{-3}, $\rho_{\text{ice}} = 916.8$ kg m^{-3}, $m_{\text{H}_2\text{O}} = 3 \times 10^{-26}$ kg, $q = 3.33 \times 10^5$ J kg^{-1}.

This demonstrates that the liquid phase of thin water layers, as described by the sandwich-model, can exist at temperatures

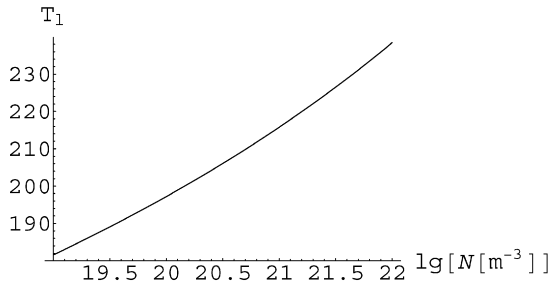

Fig. 7. Dependence of the limiting temperature T_l of the liquid phase of the water layer in the sandwich-model on the equilibrium water vapor number density (pressure).

far below the bulk melting temperature of water. The liquid water below the freezing point temperature corresponds to the unfrozen water, mentioned above, as it is characteristic for soil- and permafrost, and as it can be of importance for physical and chemical processes in the upper surface of Mars.

It is interesting to note that the limiting temperature of the liquid phase is around or below 200 K under martian conditions assuming mid- and low-latitudinal number densities of the atmospheric water molecules in the range around 3×10^{19} m^{-3} (or 10 pr μm). The presence of an average column water content of about 10 pr μm or more in the martian surface (Smith, 2004) indicates that the liquid interfacial water can exist in the upper surface in equilibrium with the atmospheric water content. There, it may have physical, rheological, chemical, and possibly also biological consequences.

4. Equilibrium moisture content of martian soil

4.1. EMC/ERH relations

The relation between equilibrium moisture content (EMC) and equilibrium relative humidity (ERH) can be described by EMC/ERH-relationships (Sun, 1998). The derived relations give the mass of the adsorbed water layer as a function of the layer height, d, and of specific surface, S_M, in a porous material of a dry mass m_{dry}:

$$M_{\text{H}_2\text{O}} = S_M m_{\text{dry}} \rho_{\text{H}_2\text{O}} d. \tag{28}$$

The EMC/ERH relation, i.e., the dependence of the equilibrium moisture content a_m on atmospheric temperature and water activity a_W is then given by

$$a_m = \frac{M_{\text{H}_2\text{O}}}{m_{\text{dry}}} = S_M \rho_{\text{H}_2\text{O}} \left(\frac{A}{6\pi (\rho_{\text{H}_2\text{O}}/m_{\text{H}_2\text{O}}) kT \left|\ln(p/p_0)\right|}\right)^{1/3}. \tag{29}$$

This relation can be applied to estimate the equilibrium water content of the upper martian surface, and vice versa. It also can give a basis to experimentally determine Hamaker's constant for ice–water–mineral systems of interest. First experimental investigations indicate, on the basis of Eq. (29) for porous materials such as chabazite, montmorillonite, clinoptilolite, and nontronite surprisingly high values of Hamaker constants in the range between 10^{-16} and 10^{-18} J (Jänchen, 2007, private communication). These relatively high values may be a

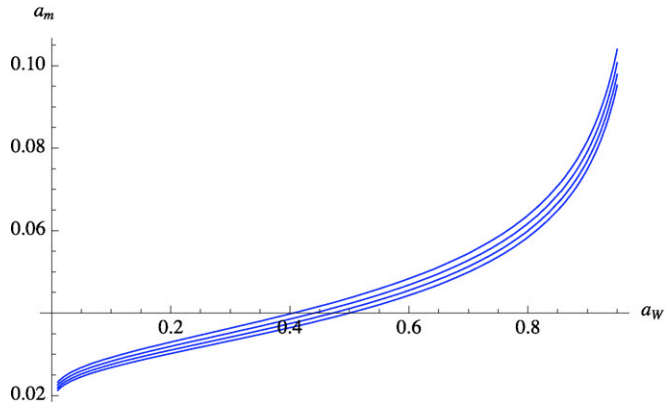

Fig. 8. Liquid water content a_m of soil in dependence on the water activity a_W (relative humidity) for temperatures of 200 (upper curve), 220, 240, and 260 K (lower curve).

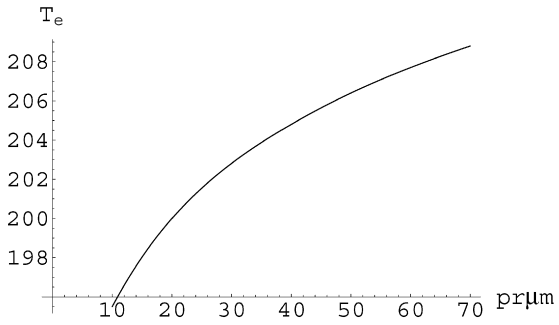

Fig. 9. Dependence of the equilibrium temperature T_e of freezing and sublimation on the atmospheric water content.

consequence of the porous structure of the minerals. This challenging result requires further investigation.

The most uncertain parameters in Eq. (29) are for Mars the specific surface, S_M and the Hamaker constant, A for relevant minerals. The $a_m(a_W)$-curve in Fig. 8 has been derived with the values $S_m = 10^5\ \mathrm{m^2\,kg^{-1}}$, and $A = 100$ zJ. Obviously, the value of the specific surface may be different in various regions of the martian surface. If the value of Ballou et al. (1978) is taken, the moisture, i.e., the soil water content, is smaller by a factor 1/6 compared to the values in Fig. 8.

These results indicate that the content of liquid water of the martian surface can for martian temperatures under equilibrium conditions reach 10% by weight and more at and around saturation (during night hours) and it is of about 2% by weight during the dry daytime hours.

4.2. *The equilibrium ice content of porous soil*

The low temperatures expected in the martian sub-surface soil indicate that water in the form of "bulk" ice in the soil is also to occur, i.e., ice, in its bulk not influenced or bound by the surfaces of the soil grains, as in the sandwich model. This ice content depends on the void space due to the porosity of the surface soil and can reach large values. It also depends, as long as there is sufficiently open (i.e., internally connected or percolative) pore space, on temperature and atmospheric water content. The equilibrium between pressure driven freezing and sublimation can be described by the equilibrium temperature, which is determined via

$$NkT_e = a\exp(-\varepsilon/kT_e). \tag{30}$$

Fig. 9 describes the dependence of T_e on the atmospheric water content (measured in pr μm). Porous and percolative sub-surface soils at equatorial- and mid-latitudes (with an atmospheric water content of around 10 pr μm) will, in diffusive equilibrium with the atmosphere, be able to temporarily condense with freezing of ice in any vacant pore spaces if the temperatures are at or below 195 K.

In the case of a porosity, $p = 0.25$ and a soil mineral mass density of 3000 $\mathrm{k\,m^{-3}}$, the ice content of the soils will be of about 10% by weight. That value may increase in the case of higher porosity. Analogously, ice can also be expected to exist on surfaces which are in shadow, over sufficiently long times, as in, e.g., deep craters or cavities, which have temperatures of or below 195 K. Slightly higher equilibrium temperatures are possible for higher atmospheric water contents (e.g., at higher martian latitudes).

Furthermore, chemically and structurally bound (Vaniman et al., 2004; Jänchen et al., 2006) water in the mineral crystals may represent as much as 10% by weight in the soil water content of the near-surface observed by the GRS instrument at low- to mid-latitudes (Feldman et al., 2002; Boynton et al., 2002; Mitrofanov et al., 2002). This local and regional content of around 10% by weight indicates in the case of porosities $p > 0.25$, the necessary existence of chemically and structurally bound water in the upper few decimeters of the martian soil. On the other hand, the thermodynamic discussion presented above shows that there must be also components of unfrozen or adsorbed water, at least temporarily. The presence of these different water components can, at present, not be determined in the observed data.

5. Conclusions

The properties of interfacial water, which is bound by van der Waals forces on grain surfaces, are described by a sandwich-model of a layer of liquid-like adsorption water between the adsorbing mineral surface layer and a premelted ice layer.

By using basic thermodynamic principles it is shown that the resulting thickness or number of mono-layers of the interfacial water depends on the Hamaker constant, on temperature, and on water activity (a measure of relative humidity). The derived equations fit well a phenomenological relation between thickness of the liquid-like layer and relative humidity, which was known earlier. Hamaker's constant for van der Waals interactions on grains and in porous media has been determined by this equation. The curvature of grain surfaces is shown to have no remarkable effects for particles in the μm-range and larger.

The application of these equations to thermo-physical conditions on Mars shows that layers of adsorbed water, which can be frozen on top, are to be expected on and in the upper surface of Mars, also at mid- and low-latitudes. These frost-layers

are shown to be equal to or smaller than a few tenths of one millimeter. This is in agreement with observations.

Another property of interfacial water layers is the freezing point depression. An equation is derived, which relates the freezing point depression to the value of Hamaker's constant, and to the latent heat of solidification, the mass density of water ice and the thickness of the liquid-like layer. Again, this equation fits well a phenomenological relation between freezing point depression and thickness of the liquid-like layer, which was known earlier. The freezing point depression can become effective down to temperatures of around 160 K. The derived equation for the lower limiting temperature of the liquid phase also depends on the water activity. This limiting temperature reaches about 180 K under conditions of an atmospheric water content of around 10 pr μm. Thus, liquid interfacial water in equilibrium with the atmospheric water content can be expected to exist in the shallow upper surface of Mars.

The water content of soil depends under equilibrium conditions on the atmospheric water content. A corresponding "Equilibrium Moisture Content" (EMC)/"Equilibrium Relative Humidity" (ERH) relation has been derived, which under equilibrium conditions allows for equilibrium conditions the derivation of the soil water content by using measurements of the atmospheric relative humidity. This indicates that the content of liquid-like water in the upper surface of Mars can temporarily reach values up to about 10% (b.w.) and more during saturation conditions while there are about 2% (b.w.) during dry daytime conditions. Furthermore, equilibrium considerations indicate for temperatures at or below the frost point a possible ice content in the range of 10% (b.w.) and more, depending on the porosity of the soil.

Acknowledgments

I am grateful to Kenneth E. Herkenhoff (USGS, Astrogeology, Flagstaff, AZ) for making me aware of the MER-Opportunity frost image (Fig. 1), and to Geoffrey A. Landis (NASA John Glenn Research Center, Cleveland, OH) for making available Fig. 1, including related mission data.

The author thanks the International Space Science Institute at Bern, Switzerland, for supporting international exchange and discussions with respect to water in the martian surface. This cooperation and support have fostered the investigations of this paper. I wish to thank Steve Clifford, and an unknown referee for their help to improve the quality of this paper, and I wish to thank my John Lee Grenfell for improving the English of the manuscript.

References

Ackler, H.D., French, R.H., Chiang, Y.M., 1996. Comparison of Hamaker constants for ceramic systems with intervening vacuum or water: From force laws and physical properties. J. Colloid Interface Sci. 179, 460–469.

Anderson, D.M., Tice, A.R., 1972. Highway Resour. Res. 373, 12.

Ballou, E.V., Wood, P.C., Wydeven, Th., Lehwalt, M.E., Mack, R.E., 1978. Chemical interpretation of Viking 1 life detection experiment. Nature 271, 644–645.

Bandfield, J.L., 2007. High resolution subsurface water ice distributions on Mars. Nature 447 (7140), 64–67.

Bish, D.L., Carey, J.W., Vaniman, D.T., Chipera, S.J., 2003. Stability of hydrous minerals on the martian surface. Icarus 164, 96–103.

Boynton, W.V., Feldman, W.C., Squyres, S.W., Prettyman, T., Brückner, J., Evans, L.G., Reedy, R.C., Starr, R., Arnold, J.R., Drake, D.M., Englert, P.A.J., Metzger, A.E., Mitrofanov, I., Trombka, J.I., d'Uston, C., Wänke, H., Gasnault, O., Hamara, D.K., Janes, D.M., Marcialis, R.L., Maurice, S., Mikheeva, I., Torkar, R., Shinohara, C., 2002. Distribution of hydrogen in the near-surface of Mars: Evidence for subsurface ice deposits. Science 297, 81–85.

Dash, J.G., Rempel, A.W., Wettlaufer, J.S., 2006. The physics of premelted ice and its geophysical consequences. Rev. Mod. Phys. 78 (3), 695–741.

Ershov, E.D., 1998. General Geocrylogy. Cambridge Univ. Press, Cambridge.

Fagerlund, 1973. Determination of pore-size distribution from freezing-point depression. Mater. Construct. 31, 215–225.

Farmer, C.B., Doms, P.E., 1979. Global and seasonal variation of water vapor on Mars and the implications for permafrost. J. Geophys. Res. 84, 2881–2888.

Feldman, W.C., Boynton, W.V., Torkar, R.L., Prettyman, T.H., Gasnault, O., Squyres, S.W., Elphic, R.C., Lawrence, D.J., Lawson, S.L., Maurice, S., McKinney, G.W., Moore, K.R., Reedy, R.C., 2002. Global distribution of neutrons from Mars: Results from Mars Odyssey. Science 297, 75–78.

Fernandez-Varea, J.M., Garcia-Moliona, R., 2000. Hamaker constants of systems involving water obtained from a dielectric function that fulfills the f sum rule. J. Colloid Interface Sci. 231, 394–397.

Hamaker, H.C., 1937. The London–van der Waals attraction between spherical particles. Physica IV 10, 1058–1072.

Jänchen, J., Bish, D.L., Möhlmann, D., Stach, H., 2006. Investigation of the sorption properties of Mars-relevant micro- and mesoporous minerals. Icarus 180, 353–358.

Jakosky, B.M., Nealson, K.H., Bakermans, C., Ley, R.E., Mellon, M., 2003. Subfreezing activity of microorganisms and the potential habitability of Mars' polar regions. Astrobiology 3, 343–350.

Jones, K.L., Arvidson, R.E., Guinness, E.A., Bragg, S.L., Wall, S.D., Carlston, C.E., Pidek, D.G., 1979. One Mars year: Viking Lander Imaging Observations. Science 204 (4395), 799–806.

Jouglet, D., Poulet, F., Milliken, R.E., Mustard, J.F., Bibring, J.-P., Langevin, Y., Gondet, B., Gomez, C., 2007. Hydration state of the martian surface as seen by Mars Express OMEGA. 1. Analysis of the 3 mm hydration feature. J. Geophys. Res. 112, doi:10.1029/2006JE002846. E08S06.

Lewis, S.R., Collins, M., Read, P.L., Forget, F., Hourdin, F., Fournier, R., Hourdin, C., Talagrand, O., Huot, J.-P., 1999. A climate database for Mars. J. Geophys. Res. 104 (E10), 24177–24194.

Landis, G.A., 2007. Observation of frost at the equator of Mars by the Opportunity rover. Lunar Planet. Sci. XXXVIII. Abstract 2423.

Liu, Z., Muldrew, K., Wan, R.G., Elliott, J.A.W., 2003. Measurement of freezing point depression of water in glass capillaries and the associated ice front shape. Phys. Rev. E 67, 62710–62722.

Mitrofanov, I., Anfimov, D., Kozyrev, A., Litvak, M., Sanin, A., Tret'yakov, V., Krylov, A., Shvetsov, V., Boynton, W., Shinohara, C., Hamara, D., Saunders, R.S., 2002. Maps of subsurface hydrogen from the high-energy neutron detector. Mars Odyssey. Science 297, 78–81.

Möhlmann, D., 2004. Water in the upper martian surface at mid- and low-latitudes: presence, state, and consequences. Icarus 168, 318–323.

Möhlmann, D., 2005. Adsorption water-related potential chemical and biological processes in the upper martian surface. Astrobiology 5 (6), 770–777.

Ryan, J.A., Sharman, R.D., 1981. H_2O frost point detection on Mars? J. Geophys. Res. 86 (C1), 503–511.

Smith, M.D., 2004. Interannual variability in TES atmospheric observations of Mars during 1999–2003. Icarus 167, 148–165.

Sneck, T., Oinonen, H., 1970. Measurements of pore size distribution of porous materials. Julkaisu State Inst. Tech. Res., Helsinki, Finland.

Sun, D.-W., 1998. Selection of EMC/ERH isotherm equations for shelled corn based on fitting to available data. Drying Technol. 16 (3–5), 779–797.

Vaniman, D.T., Bish, D.L., Chipera, S.J., Fialpis, C.I., Carey, J.W., Feldman, W.C., 2004. Magnesium sulfate salts and the history of water an Mars. Nature 431, 663–665.

Wettlaufer, J.D., Worster, M.G., 2006. Premelting dynamics. Annu. Rev. 38, 427–452.

Wheeler, A., 1955. Catalysis. 2. Fundamental Principles. Reinhold Publ. Corp., New York.

Wilen, L.A., Wettlaufer, J.S., Elbaum, M., Schick, M., 1995. Dispersion-force effects in interfacial premelting of ice. Phys. Rev. B 52 (16), 12426–12433.

Williams, P.J., Smith, M.W., 1989. The Frozen Eart. Cambridge Univ. Press, New York, 306 pp.

Wood, S.E., Battino, R., 1990. Thermodynamics of Chemical Systems. Cambridge Univ. Press, Cambridge.

Zent, A.P., Quinn, R.C., 1997. Measurement of H_2O adsorption under Mars-like conditions: Effects of adsorbent heterogeneity. J. Geophys. Res. 102 (E4), 9085–9096.